Energy Reports 15 (2026) 109349

Contents lists available at ScienceDirect

Energy Reports

journal homepage: www.elsevier.com/locate/egyr

Research paper

Developing mission profiles for lifetime assessment of bidirectional AC charging on electric vehicle power electronics☆

Stefan Schmalzl [a], Michael von Bonin [b], Michael Frey [a,*], Frank Gauterin [a], Martin Braun [b,c]

[a] Institute of Vehicle System Technology, Karlsruhe Institute of Technology (KIT), Rintheimer Querallee 2, 76131, Karlsruhe, Germany
[b] Fraunhofer Institute of Energy Economics and Energy System Technology IEE, Joseph-Beuys-Str. 8, 34117, Kassel, Germany
[c] Department of Sustainable Electrical Energy Systems, University of Kassel, Wilhelmshöher Allee 73, 34121, Kassel, Germany

ARTICLE INFO

Keywords:
Electric mobility
Mission profiles
Bidirectional charging
Powerelectronics
Onboard charger
Lifetime impact
Charging profiles
Feed-in profiles
Charging optimization
Sensitivity analysis
Energy market
Solar charging
Model validation

ABSTRACT

The bidirectional charging of electric vehicles offers new opportunities to create value streams that can reduce total cost of ownership. While research has largely focused on high-voltage battery aging, less attention has been paid to power electronic components, such as the onboard charger, whose premature failure can result in substantial repair costs. This study develops high-fidelity mission profiles for bidirectional AC charging using a validated simulation model that accurately reproduces real-world field data. The mission profiles, defined as time-dependent sequences of electrical and thermal stresses experienced by power-electronic components during operation, are derived for electric vehicles in households equipped with a photovoltaic system under two operating scenarios: one with a large cost feed-in price spread, where self-consumption dominates, and one with a small price spread, enabling market-driven energy trading. Energy exchange optimization is conducted in the German Day-Ahead and combined Day-Ahead/Intraday markets. Results show that bidirectional charging substantially increases energy throughput, operating hours, and switching events of power-electronic components, with vehicle availability and annual driving distance being key factors. Sensitivity analysis further highlights that battery state-of-charge limits, auxiliary losses from cooling and communication controllers, and grid-imposed feed-in power constraints strongly affect achievable feed-in energy. The increased number of charging and switching events amplifies thermal cycling and cumulative stress on the onboard charger. For the scenarios considered, using a bidirectional electric vehicle as a mobile energy storage system can yield net savings of up to approximately 400 € per year on the household electricity bill in Germany. The developed mission profiles provide a robust foundation for component lifetime assessment and support the development of control strategies that balance profitability with component durability.

1. Introduction

The electrification of mobility continues to accelerate. More than 58 million electric vehicles are now on the worldwide roads, with 17 million added in 2024. This marks a 25% annual increase compared to 2023. A closer look on the powertrain technology split reveals a strong preference for battery electric vehicles (BEVs), accounting for 64% of the global yearly electric vehicle sales in 2024 (International Energy Agency (IEA), 2025). BEVs not only offer higher driving efficiency than internal combustion engine (ICE) vehicles, but they can also serve as energy storage devices when equipped with bidirectional charging capabilities. Two factors support the use of the HV battery beyond mobility. First, the battery capacity is often larger than what is needed for daily mobility. Second, private cars spend the vast majority of their time unused, remaining parked for up to 95% of a day (Nagler, 2021). When connected to the grid, a portion of the battery capacity could be used to provide value-added services, thereby reducing the vehicle's total cost of ownership. The literature highlights numerous bidirectional charging use cases, including vehicle-to-load (V2L), vehicle-to-home (V2H), vehicle-to-building (V2B) or vehicle-to-grid (V2G). Prominent examples for V2G use-cases include congestion management, voltage control, frequency control or reactive power control (Banol Arias et al., 2019). The review articles Yilmaz and Krein (2012) and Rodriguez et al. (2021) provide a comprehensive overview of the advantages and potential limitations of V2G services. Recent

☆ This work was supported by the German Federal Ministry for Economic Affairs and Climate Action (BMWK) under the projects "EMob-Cold+V2G" (grant number 16EM7001) and "Ladeinfrastruktur 2.0" (grant number 0350048D).

* Corresponding author.
E-mail address: michael.frey@kit.edu (M. Frey).

https://doi.org/10.1016/j.egyr.2026.109349
Received 7 November 2025; Received in revised form 20 March 2026; Accepted 21 April 2026
Available online 29 April 2026

household-centric optimization studies have further analyzed bidirectional operation with respect to market integration, smart-home use cases, and profitability (Dargahi et al., 2014; Kern et al., 2020, 2022; Vollmuth et al., 2024; Popolizio et al., 2025). However, these studies predominantly report aggregate outputs such as cost savings, self-consumption, state-of-charge trajectories, and exchanged energy, rather than reliability-relevant mission-profile descriptors such as power-level distributions, event durations, and operating-hour statistics. Among the frequently discussed limitations of bidirectional charging is its potential negative effect on component lifetime. As a result, extensive research has been conducted on the impact of bidirectional charging on HV battery longevity. For instance, Dubarry et al. (2017) and Sagaria et al. (2025) investigated the effects on commercial lithium-ion cells used in electric vehicles, discovering that lifetime is affected, with cyclic degradation being the most critical factor. However, recent experimental studies suggest that the challenge of accelerated battery aging may be less severe than previously assumed and offer recommendations for optimal charging and discharging strategies (Gong et al., 2024). Although battery aging has been extensively studied, the impact of bidirectional charging on BEV power electronics remains largely underexplored. Changes in mission profiles, such as extended operating hours, can accelerate the aging of components, potentially requiring their replacement before the vehicle reaches the end of its service life. The substantial effort involved in such replacements can lead to significant costs, potentially offsetting the benefits of bidirectional charging. Moreover, the ongoing trend toward mechanical and functional integration of power electronic components in BEVs may further complicate repairs, underscoring the need for a detailed understanding of how bidirectional charging affects power electronics (Pradhan et al., 2023; Kim and Park, 2024).

The literature contains numerous studies investigating aging effects on power electronic systems. However, the vast majority of these works focus on stationary applications, such as inverters for wind turbines (Ma et al., 2015; Zhou et al., 2019) or solar systems (De León-Aldaco et al., 2013; Lenz et al., 2017). In contrast, research on power electronic components of BEVs, remains limited. For example, Hirschmann et al. (2007) and Soldati et al. (2018) developed modeling approaches for reliability studies of traction inverters, while Chakraborty et al. (2022) introduced a model to investigate a HV DC/DC converter. An exemplary modeling of a traction inverter and an onboard charger is presented in Blaabjerg et al. (2021). These studies primarily focus on the aging effects of semiconductors and capacitors, which are more likely to cause component failures (Yang et al., 2009). In practical onboard chargers, dominant wear-out risks are often associated with power semiconductors (bond-wire and solder fatigue due to thermal cycling) and DC-link capacitors (temperature- and ripple-current-driven aging), while magnetic components can also become critical under sustained high-current operation. Lifetime studies are often customized to specific onboard charger topologies, semiconductor types, capacitor selections, and cooling concepts. Reliability-oriented charger lifetime studies do exist, but they typically evaluate stylized charging and discharging profiles rather than household-optimized mission profiles (Polat et al., 2023). This study seeks to lay a foundational groundwork for future research by presenting a methodology and creating bidirectional mission profiles that can be used to investigate the lifetime impact of bidirectional charging on power electronic components. At present, the scientific literature offers no comprehensive overview of the key characteristics of such mission profiles as well as their sensitivity to modeling parameters. Most studies touching mission profiles focus on specific aspects, such as additional energy exchange or remuneration, with notable contributions by Kern et al. (2020) and Vollmuth et al. (2024). In contrast to those studies, this work explicitly derives reliability-relevant mission-profile descriptors, including power-level distributions, event durations, and operating-hour patterns, and links them to scenario assumptions. Additionally, many studies simplify modeling by excluding DC charging events, assuming that annual energy intake occurs solely through AC charging. To the authors' knowledge, this is the first study to generate bidirectional AC charging mission profiles that incorporate charging and feed-in power distributions, event duration, and the relationship between accessible additional operating hours from bidirectional charging and annual mileage. The main contributions of this article include:

- A validated methodology to generate yearly bidirectional AC charging mission profiles for EV power-electronic lifetime studies, benchmarked against field data from 18 BEVs and extended with DC charging events for realistic annual AC-energy estimation.
- A scenario-based mission-profile analysis (unidirectional, solar-optimized, bidirectional) resolving reliability-relevant descriptors such as power distributions, event durations, operating hours, and ambient-temperature exposure.
- A sensitivity and profitability assessment quantifying how SoC constraints, auxiliary losses, grid limits, and market design shape feed-in energy and annual savings.

For this study, energy prices from the German electricity market are used, while the methodology is fully transferable to other markets. The remainder of the paper is structured as follows: Section 2 introduces the lifetime assessment framework for power electronic components. Section 3 outlines the methodology for generating mission profiles. Section 4 presents model validation using real-world data. Sections 5–7 detail the results of mission profile generation, the energy bill savings from energy feed-in, and the sensitivity analysis. Section 8 concludes the paper and provides an outlook on future research.

To ensure broad applicability, this study focuses on the generation of bidirectional AC charging mission profiles rather than on component-level lifetime impacts. Component specific electro-thermal simulations are deliberately omitted, as quantities such as ΔT_j are inherently tied to semiconductor packaging, cooling, and power electronic topology. By focusing on transferable mission profiles rather than absolute lifetime metrics, the study provides a versatile stochastic framework that serves as a foundation for subsequent hardware-specific modeling.

2. Lifetime assessment

Power electronic components are subject to a variety of factors that influence their likelihood of failure. To analyze these factors in a structured way, it is useful to categorize them according to the phases of the product life cycle. In this context, the Weibull failure rate Eq. (1) is introduced, providing a mathematical description of how the failure rate of power electronic components evolves over time. The equations underlying parameters include the shape parameter β, which defines the curve shape, the scale parameter μ, representing the components characteristic life and γ, known as the location parameter or failure-free lifetime. By utilizing the shape parameter β, the product lifetime can be partitioned into three phases, indicated by the dashed lines in Fig. 1. The range $\beta < 1$ describes early product failures, which decrease with increasing product testing and field experience. The range $\beta = 1$ corresponds to useful product life, where product failures occur stochastically and only at a constant but low failure rate. The range $\beta > 1$ represents product failures caused by wear-out. It is highlighted in red, as the study focuses on this phase. Due to its characteristic shape, the representation of the Weibull failure rate across these three phases is commonly referred to as the Bathtub curve (Lienig and Bruemmer, 2017).

$$\lambda(t) = \frac{\beta}{\mu}\left(\frac{t-\gamma}{\mu}\right)^{\beta-1} \quad t \geq \gamma, \quad \beta, \mu \in \mathbb{R}^+ \quad t, \gamma \in \mathbb{R} \tag{1}$$

Fig. 2 illustrates a typical lifetime assessment framework for a semiconductor power module within an EV onboard-charger. The red box highlights the mission profile, while the two dashed boxes represent the component simulation model and the lifetime assessment model. As this study does not delve into a detailed evaluation of a specific component,

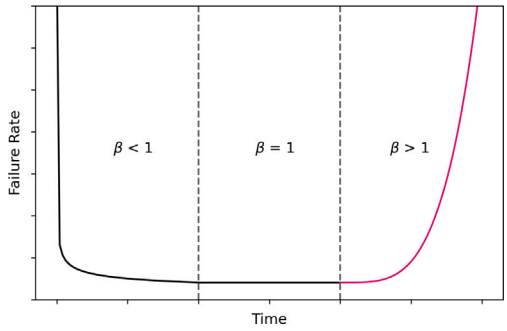

Fig. 1. Weibull failure rate for different shape parameters. Early product failures: $\beta < 1$, constant or stochastic product failures: $\beta = 1$, wear-out failures: $\beta > 1$. The study focuses on wear-out failures.

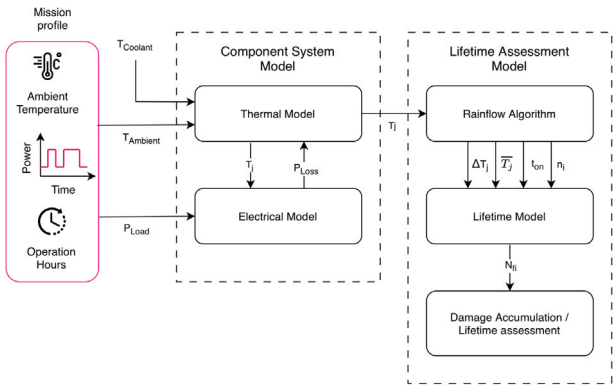

Fig. 2. Lifetime assessment model of a semiconductor power module within an EV onboard charger. The red box indicates the scope of this paper: the development of representative mission profiles for bidirectional AC charging (Novak et al., 2020).

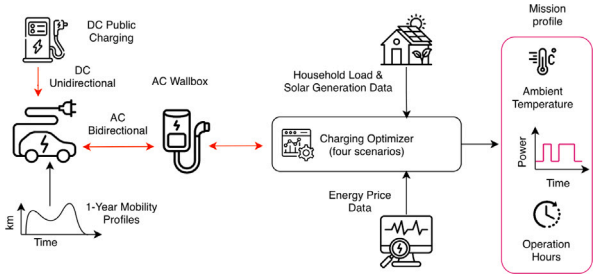

Fig. 3. Overview simulation framework showing the optimization process and input data for generating bidirectional AC mission profiles. BEV energy exchange occurs bidirectionally via AC at home or work, based on one-year mobility profiles and charging strategy, or unidirectionally via DC for long-distance trips.

the assessment process is only briefly summarized. For more details, please refer to Novak et al. (2020) and Kardan et al. (2023).

For a comprehensive lifetime assessment, a mission profile must deliver two essential pieces of information. First, it should include a load profile that outlines the relative distribution of charging power along with the corresponding operating hours. Second, it must detail the thermal environmental conditions, such as ambient temperature T_{amb} and coolant temperature T_{coolant}. The evaluation process commences by feeding the mission profile into the component simulation model. The interaction between the electrical and thermal component models results in the temporal evolution of the junction temperature T_j of the semiconductors. The temporal evolution of the junction temperature is then analyzed within the lifetime assessment model using the Rainflow algorithm. This algorithm extracts critical parameters, including the mean junction temperature $\overline{T}_j$, junction temperature swings ΔT_j, heating time t_{on}, as well as the actual number of cycles n_i the component experiences at stress level i during its operation. These parameters are subsequently fed into an empirical lifetime model of the semiconductor power module, which calculates the number of cycles to failure N_{fi} based on the current stress level i. Finally, the fraction of consumed life C of the semiconductor power module is determined, for example, by using Palmgren–Miner's linear damage accumulation model, illustrated by Eq. (2) (Miner, 1945). The lifetime model is specific to each semiconductor power module and it can be derived, for instance, through power cycling tests. The subsequent sections develop these mission profiles to parameterize the red box in Fig. 2, enabling future component-level assessments.

While the Weibull distribution conceptually describes the progression toward the wear-out regime ($\beta > 1$), a quantitative reliability assessment requires both the mission profiles developed in this work and hardware-specific lifetime parameters. This analysis establishes the mission profiles necessary to serve as input for such models upon the availability of calibrated component data. Accordingly, Eqs. (1) and (2) are presented as the governing conceptual framework.

$$C = \sum_i \frac{n_i}{N_{fi}} \tag{2}$$

3. Mission profile generation

Fig. 3 illustrates the optimization framework alongside the input data used to create bidirectional AC mission profiles. The BEVs energy exchange can occur either bidirectionally via AC or unidirectionally via DC. Bidirectional AC charging is possible at home or at the workplace, depending on vehicle availability, which is determined by one-year mobility profiles and the selected charging strategy. DC fast charging is primarily utilized during long-distance trips due to its higher cost. The following sections offer a detailed explanation of the input data for the optimization framework.

The focus on bidirectional AC for residential operation mainly affects converter-level efficiency and thermal-stress interpretation, because the power-conversion stage is located in the onboard charger rather than in a DC wallbox. In contrast, the availability windows (arrival, departure, and parking duration) are driven by mobility behavior and are therefore modeled independently of AC/DC converter placement. Consequently, the presented mission profiles are directly representative for AC bidirectional home charging, while transfer to DC-centric residential setups should be interpreted primarily at the level of operational patterns rather than absolute converter stress levels.

3.1. Mobility module

Mobility data is derived as probability density functions (PDFs) from the survey "Mobilität in Deutschland" (MiD) (Infas Institut für Sozialwissenschaft, 2018). This survey is a representative survey of mobility behavior in Germany, providing detailed information on vehicle usage, including daily mileage, trip duration, trip purpose, as well as user and household data such as income, household size, and geographical information. Since MiD was collected in a mixed-fleet context rather than an EV-only sample, it is used here to parameterize temporal mobility and availability behavior, not EV technology shares. In addition, key indicators were cross-checked and updated using the latest MiD publication (2023 release) (Infas Institut für Sozialwissenschaft, 2023) to improve consistency with current mobility statistics. By combining socioeconomic data with mobility data, representative data for specific user groups can be generated. The PDFs are used to generate mobility profiles for three different geographical regions: metropolitan (R1), suburban (R3), and rural (R7). For each area, a random selection of 100

Table 1
Mobility statistics for Germany and various regions: R1 = Metropolitan City Region, R3 = Urban Region or Medium-Sized City, R7 = Rural Region.

	Germany	R1	R3	R7
Total share	100%	19.71%	24.72%	14.62%
Non-car commuting	0.31	0.49	0.25	0.18
Travel car	0.86	0.93	0.84	0.80
Annual mileage in km	13 330	12 428	13 359	14 841
Travel distance in km	1694	2148	1706	1276
Everyday distance in km	11 636	10 280	11 652	13 566
Travel trips per Year	2.25	2.72	2.19	1.72
Commute distance in km	14.71	13.79	15.00	17.46
Travel days	10.27	11.62	9.88	9.31

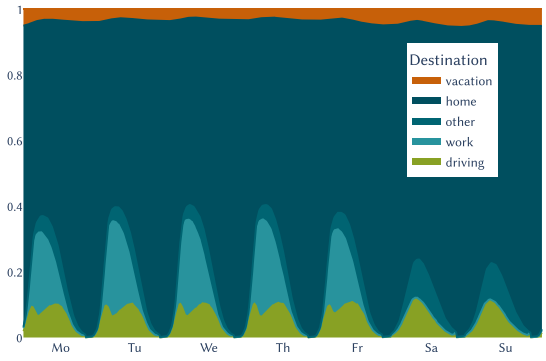

Fig. 4. Probability Density Location for a representative sample of 500 profiles in a suburban area.

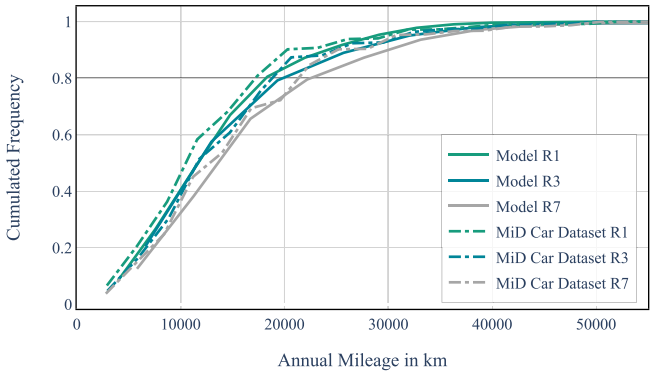

Fig. 5. Validation of annual mileage distribution.

Table 2
Key factors impacting mobility behavior.

Factor	Description
Socio-economic changes	Shifts in employment, remote work, and urbanization affecting travel frequency and duration.
Impact of COVID-19	Pandemic-driven increase in telecommuting and reduction in travel demand.
Changing consumer preferences	Greater environmental awareness driving sustainable transport and shared mobility adoption.
Long-term trends	Continued influence of telecommuting, evolving urban planning, and emerging technologies such as autonomous driving.

profiles is generated. The profiles are generated for a one-year period with a 15-minute time resolution, encompassing information on vehicle location, trip duration, and trip purpose. The households are randomly selected from the MiD survey. Each day is generated randomly based on the PDFs, while some user-specific patterns are preserved across days to reflect realistic mobility behavior. For instance, persons consistently maintain the same commuting distance, ensuring that habitual travel patterns, such as commuting routines, are preserved while allowing for daily and seasonal variations. Moreover, the travel dataset and statistics consider seasonal variations that influence mobility behavior, affecting trip frequencies and distances, which subsequently impact energy and charging demand. Table 1 presents key statistics for different geographical regions to underscore fundamental differences. For instance, the total share of non-car commuting is significantly higher in the metropolitan area (R1) compared to the rural area (R7).

Fig. 4 depicts the average location of vehicles over the modeled period, closely aligning with the distribution reported in the MiD results. On average, only about 3 percent of vehicles are actively on the road at any given time. Even during peak hours, no more than 10 percent of vehicles are simultaneously in motion. Analyzing the data over an entire week reveals a consistent trend: more than half of all vehicles remain parked at home during any given period. Additionally, a significant portion, up to 30 percent, are located at workplaces during standard work hours on weekdays.

Fig. 5 illustrates the distribution of annual mileage across the three geographical regions included in the modeled dataset, compared to the corresponding data from the MiD 2017 vehicle survey. The results indicate that the generated profiles closely mirror the driving behavior of German vehicle users. The slight deviation in the cumulative distribution function (CDF) can be attributed to methodological biases in the MiD survey, which tends to underrepresent high-mileage drivers. This discrepancy may result from factors such as self-reporting inaccuracies or sample composition effects, leading to a lower proportion of frequent long-distance drivers being captured in the survey. Despite this minor deviation, the overall alignment of the modeled data with the survey results suggests that the synthetic vehicle usage profiles provide a robust representation of real-world driving patterns in Germany. However, since the MiD survey was conducted in 2017, socio-economic and infrastructural developments have taken place that continue to shape mobility behavior. These shifts may not be fully reflected in the original dataset. Consequently, transferability to 2026 is strongest for relative scenario effects and usage-pattern trends, while absolute annual values should be interpreted with appropriate caution. Table 2 summarizes the main factors and their implications.

3.2. Electric vehicle module

To evaluate the impact of EV model selection, four electric vehicles with different vehicle and charging parameters are examined, as detailed in Table 3. The usable battery capacities range from 38 kWh to 98 kWh, providing a wide spectrum for analyzing the utilization of both larger and smaller HV batteries. For realistic energy consumption modeling, the vehicle's energy consumption during driving is represented as a constant average over multiple trips, with additional energy consumption for auxiliaries, like heating or air conditioning. Within the temperature range of −10 °C to 40 °C, the vehicles average total energy consumption can be approximated using a quadratic function, as shown in Fig. 6. This modeling is based on a validated measurement campaign, with further details available in Koncar and Bayram (2021). Table 4 presents the quadratic fit parameters. The vehicle parameters are sourced from Electric Vehicle Database (2025).

3.3. Household loadprofile module

This study explores various charging strategies, including self-consumption-optimized charging with a solar roof. For this purpose, a representative household load profile is modeled over one year based on a dataset comprising 74 measured household load profiles (Tjaden et al., 2015). The dataset's annual energy consumption ranges from 1400 to 8600 kWh, with a median of 4700 kWh,

Table 3
Electric vehicle parameter. A: Useable High-Voltage Battery Capacity [kWh], B: AC Charging Power [kW], C: Average DC Charging Power (10%–80%) [kW].

Vehicle Model	A	B	C
Tesla Model 3 SR Plus	49.0	11.0	105.0
Tesla Model 3 LR	72.0	11.0	108.0
Tesla Model S LR Plus	98.0	16.5	125.0
BMW I3	38.0	11.0	47.0

Table 4
Quadratic fit parameters for EVs average total energy consumption for driving and auxiliaries($E = aT^2 + bT + c$). E = EVs average total energy consumption for driving and auxiliaries [Wh/km], T = Temperature [°C].

Vehicle Model	a	b	c
Tesla Model 3 SR Plus	0.0517	−2.17	150.19
Tesla Model 3 LR	0.0550	−2.31	157.83
Tesla Model S LR Plus	0.0519	−2.44	177.90
BMW I3	0.0535	−2.27	161.98

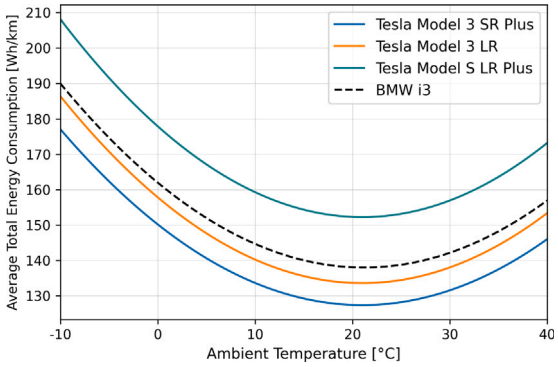

Fig. 6. EVs average total energy consumption for driving and auxiliaries versus ambient temperature for the studied vehicle models. The quadratic fit is based on data from a measurement campaign (Koncar and Bayram, 2021).

which typically corresponds to a four-person household and reflects the typical electricity demand of battery electric vehicle (BEV) households with rooftop PV, where self-consumption ratios of 20%–40% are common (for Solar Energy Systems ISE, 2024). More recent household datasets increasingly embed additional new electric loads and PV-related effects. In this work, these effects are modeled explicitly in separate modules, so using the 2015 household dataset helps avoid double counting while preserving robust baseline temporal consumption patterns. The statistical distribution for workdays, Saturdays, and Sundays is depicted in Fig. 7.

3.4. Photovoltaic generation module

To analyze self-consumption-optimized charging with a solar roof, annual PV generation profiles are created using a PV time series generator developed by Fraunhofer IEE. These profiles cover nine different German cities. Berlin, Hamburg, Cologne, Frankfurt, Stuttgart, Düsseldorf, Leipzig, Dortmund, and Hannover, with three potential roof orientations: south, southwest, and southeast. The solar roofs have peak capacities ranging from 3.0 kWp to 19.6 kWp, with an average of 8.2 kWp. Further details on the profile generation process can be found in Böttger et al. (2019). Fig. 8 illustrates the median of the PV generation profiles along with the 25% and 75% quantiles for the

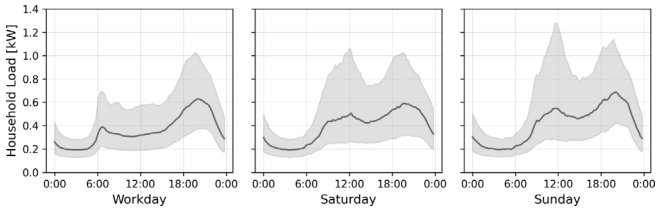

Fig. 7. Statistical distribution of household load profiles for workdays, Saturdays, and Sundays. The yearly median consumption is 4700 kWh. The solid line denotes the median, while the shaded areas represent the 25th–75th percentiles (Tjaden et al., 2015).

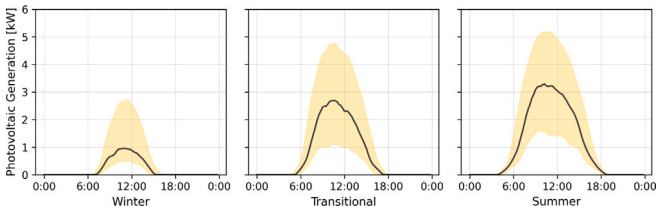

Fig. 8. Photovoltaic generation profile median and 25% and 75% quantiles for winter, transitional and summer period. The time periods align with those of the H0 standard load profile (BDEW Bundesverband der Energie- und Wasserwirtschaft e.V., 2025).

Table 5
Day-Ahead energy price statistic for 2021 and 2024.

Year	Average daily mean [€]	Average daily std. [€]
2021	0.330	0.029
2024	0.406	0.037

Table 6
Intraday-Auction energy price statistic for 2021 and 2024.

Year	Average Daily Mean [€]	Average Daily Std. [€]
2021	0.330	0.035
2024	0.408	0.046

winter, transitional, and summer periods. The time periods correspond to those of the H0 standard load profile (SLP) (BDEW Bundesverband der Energie- und Wasserwirtschaft e.V., 2025).

3.5. Energy price module

The charging prices are derived from EEX market data of 2021 and 2024 (EEX, 2025). The analysis includes both the Day-Ahead and Intraday markets. Price data is adjusted to account for grid fees and taxes, ensuring realistic end-user prices (see Tables 5 and 6). Fig. 9 illustrates exemplary price data for a period from Friday to Monday in 2021.

The subsequent analyses in the results section are conducted for 2021, exploring two distinct scenarios. The first Variant Assumes that feed-in consumption is compensated solely at the wholesale market price, resulting in a relatively large average consumption–feed-in price spread of 233 €/MWh. In the second scenario, taxes and levies paid on consumption are reimbursed upon feed-in, so that only a residual difference of 3.5 €/MWh remains to cover the trader's costs and margin. This markup is derived from Purkus et al. (2015).

3.6. Ambient temperature module

The study investigates whether charging events statistically correspond with the ambient temperature distribution or if they show

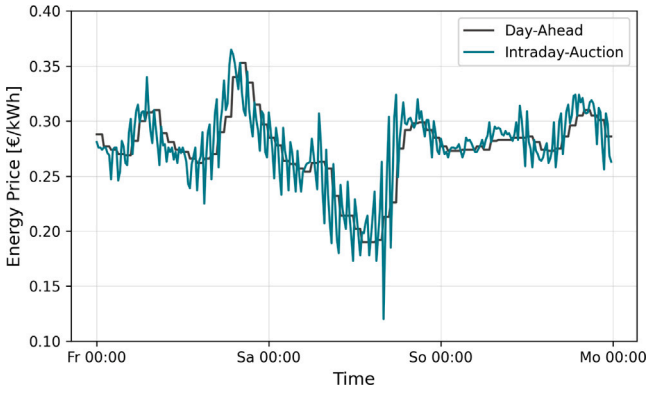

Fig. 9. Exemplary Day-Ahead and Intraday EEX market data for a time period from Friday to Monday in 2021. Price data is adjusted to account for grid fees and taxes.

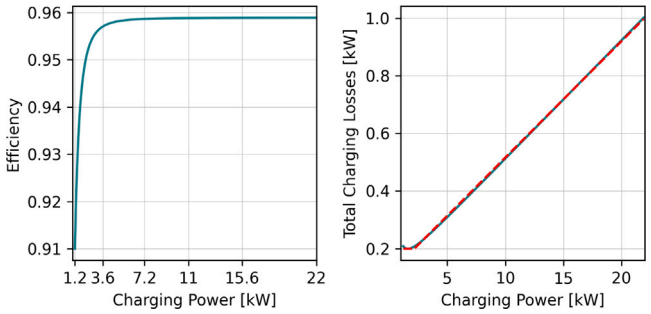

Fig. 10. Charging efficiency for state-of-the art automotive AC onboard chargers (Pham et al., 2022). Total charging losses, accounting for the AC onboard charger efficiency and an additional 100 W auxiliary losses from the coolant pump, charging communication controller, and charging control unit (Wouters and Martinez, 2024). The dashed line represents a piecewise linear fit of the losses.

systematic deviations due to specific charging strategies. For this analysis, temperature data from 2021 from the Stuttgart-Echterdingen weather station with the station ID 4931 is used (DWD, 2025). Ambient temperature is explicitly used to evaluate the temperature distribution of charging and feed-in events and to parameterize temperature-dependent driving-energy demand in the vehicle module. However, the model does not include an explicit dynamic coolant-temperature model for the onboard charger.

3.7. Charging efficiency

The charging efficiency used in this study is illustrated in Fig. 10, representing values typical of a state-of-the-art AC onboard charger (Pham et al., 2022). The high efficiencies at partial loads are achieved through phase deactivation. Single-phase charging can deliver up to 3.6 kW, two-phase charging up to 7.2 kW, and three-phase charging operates above 7.2 kW.

The same figure also presents the total charging losses, calculated from the AC onboard charger efficiency combined with additional auxiliary losses of 100 W. These auxiliary losses account for energy consumed by the water coolant pump, the charging communication controller, and the charging control unit. The 100 W value is based on Wouters and Martinez (2024), which reports auxiliary losses in the range of 100–450 W. It is assumed that future vehicles can achieve the lower end of this range, but the effect of higher base losses is explored in the sensitivity analyses.

Within the optimization model, charging losses are approximated using a piecewise linear function, as indicated by the red dashed line. Charging or feed-in is assumed not to be initiated below 0.3 kW due to technical limitations. Between 0.3 kW and 2.5 kW, losses are modeled as constant, while above 2.5 kW, losses increase linearly. Neglecting a minimum charging or feed-in power of 0.3 kW would allow unrealistically low power levels, which are not feasible for real AC onboard chargers. For profitability assessment, temperature effects are therefore captured indirectly through temperature-dependent mobility energy demand and the ambient-temperature distribution of charging/feed-in events, while explicit temperature-dependent feed-in efficiency and coolant control dynamics are outside the scope of the present optimization model.

3.8. Optimization

The optimization model determines the cost-optimal scheduling of household electricity flows, including photovoltaic generation, consumption, and bidirectional vehicle charging. Its objective is to minimize the household's net annual energy costs by dynamically allocating charging, discharging, and grid exchange over time. The mixed-integer linear program (MILP) therefore decides in each hourly timestep whether the electric vehicle should charge from the grid, supply energy back to the household or grid, or remain idle, considering electricity prices, photovoltaic availability, and vehicle availability constraints. Technical limits such as charging power, state-of-charge boundaries, and grid feed-in restrictions are explicitly incorporated to ensure realistic operation.

For clarity, AC and DC charging are represented in one unified optimization formulation, but with different availability domains. AC charging and feed-in variables are active only when the vehicle is parked at a location with charging access (home and, if enabled by scenario, workplace). DC charging is restricted to mobility timesteps associated with long-distance travel demand and is not used for routine household energy arbitrage. This joint formulation is used to avoid overestimating AC charging availability over the year while preserving a consistent battery-energy balance across home charging and en-route charging events.

The cost-optimal bidirectional energy exchange is determined by solving a Mixed Integer Linear Programming optimization problem. The cost function (3), consists of multiple terms. The first two represent the total AC energy consumption $J_{E,n}^{AC^+}$ from the power grid and the AC energy feed-in $J_{E,n}^{AC^-}$ into the power grid. Additional terms model the electric vehicles DC energy consumption $J_{E,n}^{DC^+}$, along further constraints formulated using Lagrange functions $J_{i,n}$ and corresponding Lagrange multipliers λ_i. The minimization problem is subject to several physical constraints, including the high-voltage battery capacity, power grid charging and feed-in limits, as well as the electric vehicles AC and DC charging capabilities. The optimization is performed over the optimization horizon $\mathcal{N}$ with each 15 min time interval represented by the parameter n.

- p^G: Grid consumption power (AC) [kW].
- p^{EV}: EV charging power (AC) [kW].
- p^{EV_L}: EV charging losses (AC) [kW].
- p^{HH}: Household consumption power [kW].
- q^G: Grid feed-in power (AC) [kW].
- q^{EV}: EV feed-in power (AC) [kW].
- q^{EV_L}: EV feed-in losses (AC) [kW].
- q^{PV}: Solar feed-in power [kW].
- z^{EV}: EV charging power (DC) [kW].
- η: Efficiency DC charging [kW].
- ϵ^+: Energy consumption cost (AC) [€/kWh].
- ϵ^-: Energy feed-in compensation (AC) [€/kWh].
- κ: DC energy consumption price [€/kWh].
- s: Travel distance [km].
- c: Energy consumption for traveling [kWh/km].
- e: EV battery energy content [kWh].

- e_{min}: EV minimum battery energy content [kWh].
- δ^i: Binary decision variables [1].
- $e\ *$: Target Battery energy content at the end of optimization horizon [kWh].

$$\begin{aligned}
\min \quad & \sum_{\substack{\forall n \in \mathcal{N} \\ \forall i \in I}} \left(J_{E,n}^{AC^+} + J_{E,n}^{AC^-} + J_{E,n}^{DC^+} + \lambda_i J_{i,n} \right) \\
\text{subject to} \quad & \underline{\mathbf{p}}^{EV} \leq \mathbf{p}^{EV} \leq \overline{\mathbf{p}}^{EV}, \quad \mathbf{p}^{EV} \in \mathbb{R}^N \\
& \underline{\mathbf{q}}^{EV} \leq \mathbf{q}^{EV} \leq \overline{\mathbf{q}}^{EV}, \quad \mathbf{q}^{EV} \in \mathbb{R}^N \\
& \underline{\mathbf{p}}^{G} \leq \mathbf{p}^{G} \leq \overline{\mathbf{p}}^{G}, \quad \mathbf{p}^{G} \in \mathbb{R}^N \\
& \underline{\mathbf{q}}^{G} \leq \mathbf{q}^{G} \leq \overline{\mathbf{q}}^{G}, \quad \mathbf{q}^{G} \in \mathbb{R}^N \\
& \underline{\mathbf{z}}^{EV} \leq \mathbf{z}^{EV} \leq \overline{\mathbf{z}}^{EV}, \quad \mathbf{z}^{EV} \in \mathbb{R}^N \\
& \underline{\mathbf{e}} \leq \mathbf{e} \leq \overline{\mathbf{e}}, \quad \mathbf{e} \in \mathbb{R}^{N+1}
\end{aligned} \tag{3}$$

The decision variables include the AC charging power of the electric vehicle p^{EV} (4), the AC feed-in power of the electric vehicle q^{EV} (5), the DC charging power of the electric vehicle z^{EV} (6) and various binary variables, which are generally denoted by δ^i (7).

$$\mathbf{p}^{EV} = \left(p_0, p_1, \ldots, p_{N-1}\right)^T \in \mathbb{R}_0^{+N} \tag{4}$$

$$\mathbf{q}^{EV} = \left(q_0, q_1, \ldots, q_{N-1}\right)^T \in \mathbb{R}_0^{-N} \tag{5}$$

$$\mathbf{z}^{EV} = \left(z_0, z_1, \ldots, z_{N-1}\right)^T \in \mathbb{R}_0^{+N} \tag{6}$$

$$\boldsymbol{\delta}^{(i)} = \left(\delta_0, \delta_1, \ldots, \delta_N\right)^T \in \{0, 1\} \tag{7}$$

The AC energy consumption term (8) consists of three components: the EVs AC charging power $p_n^{EV} \geq 0$, the EVs charging losses $p_n^{EV_L} \geq 0$ and the household power consumption $p_n^{HH} \geq 0$. Together, these contribute to the total power consumption from the grid $p_n^G \geq 0$. The cost associated with AC energy consumption is represented by the AC energy consumption price ϵ_n^+.

$$J_{E,n}^{AC^+} = \underbrace{\left(p_n^{EV} + p_n^{EV_L} + p_n^{HH}\right)}_{p_n^G} \cdot \epsilon_n^+ \cdot \Delta t \tag{8}$$

The AC energy feed-in term (9) is defined by three components: the EV's AC feed-in power $q_n^{EV} \leq 0$, the EV's feed-in losses $q_n^{EV_L} \geq 0$ and the power feed-in from the PV system $q_n^{PV} \leq 0$. Together, these contribute to the total power fed into the grid $q_n^G \leq 0$. The power feed-in is compensated by the AC feed-in price ϵ_n^-.

$$J_{E,n}^{AC^-} = \underbrace{\left(q_n^{EV} + q_n^{EV_L} + q_n^{PV}\right)}_{q_n^G} \cdot \epsilon_n^- \cdot \Delta t \tag{9}$$

The DC charging term (10) is represented by the DC charging efficiency η, the EVs DC charging power z_n^{EV}, and the DC charging costs κ_n. The DC charging costs are assumed to be a constant 0.64 €/kWh.

$$J_{E,n}^{DC} = \frac{1}{\eta} \cdot z_n^{EV} \cdot \kappa_n \cdot \Delta t \tag{10}$$

In addition to the charging and feed-in terms, three Lagrange functions are formulated. The first Lagrangian function J_1 (11) imposes a penalt, when the battery energy content falls below the minimum threshold. If the high-voltage battery energy level e drops below e_{min}, the binary variable $\delta^{(1)}$ is forced to 1 by the inequality constraint (12). By the summation of J_1 in the cost function, the number of instances where e_{min} is violated is minimized.

$$J_1 = \delta^{(1)} \tag{11}$$

$$\frac{e_n - e_{min}}{\overline{e}} \geq -\delta_n^{(1)} \tag{12}$$

The second Lagrangian function J_2 (13) ensures that at the end of the optimization horizon $\mathcal{N}$, the energy content of the EV high-voltage battery e_N is greater than or equal to the target energy level e^*.

$$J_2 = \delta_n^{(2)} \tag{13}$$

$$\delta_n^{(2)} \geq e^* - e_N \tag{14}$$

The third Lagrangian function J_3 (15) ensures that DC charging sessions are completed as quickly as possible. To achieve this, the binary variable $\delta^{(3)}$ is introduced, which is set to 1 if $z_n^{EV} > 0$ and 0 otherwise. This is implemented using the big-M method (16).

$$J_3 = \delta^{(3)} \tag{15}$$

$$z_n^{EV} \leq M \cdot \delta^{(3)} \tag{16}$$

AC charging and feed-in losses are modeled using piecewise-linear functions. Charging powers below 0.3 kW are considered technically infeasible, losses remain constant between 0.3 kW and 2.5 kW, and increase linearly above 2.5 kW. The piecewise-linear modeling is implemented using additional binary variables δ. The state variable e is updated based on the charging and discharging processes of the electric vehicle, following Eqs. (17) and (18).

$$e_{n+1} = e_n + \Delta e_n \tag{17}$$

$$\Delta e_n = \left(p_n^{EV} + q_n^{EV} - p_n^{EV_L} - q_n^{EV_L} + \eta \cdot z_n^{EV}\right) \cdot \Delta t - c_n \cdot s_n \tag{18}$$

The AC energy balancing Eq. (19) ensures that the balance between energy consumption and feed-in is maintained at all times.

$$p_n^G + q_n^G = p_n^{EV} + p_n^{EV_L} + p_n^{HH} + q_n^{EV} + q_n^{EV_L} + q_n^{PV} \tag{19}$$

The optimization is performed over a 3-day window with a 15-minute resolution. After each run, only the results from the first day are retained, and the window is advanced by one day. This rolling horizon approach is employed to align with current European market mechanisms, where Day-Ahead and Intraday price signals provide a maximum look-ahead of approximately 36 h. After each execution, only the results from the first 24 h are retained to mitigate terminal boundary effects. Extending the optimization horizon beyond the 3-day window is not expected to materially reshape lifetime-critical stress sequences. In the context of bidirectional AC charging, the clustering of operational events is primarily driven by price volatility and vehicle availability. While narrow connection windows could theoretically lead to stress clustering where power exchange is compressed into high-intensity bursts, empirical mobility data suggests that parking durations available for bidirectional AC charging provide sufficient flexibility to distribute energy transfer, ensuring that the generated mission profiles reflect realistic operational conditions rather than optimization-induced artifacts.

When optimization in both the Day-Ahead and Intraday markets is targeted, a two-step approach is applied. First, optimization is performed in the Day-Ahead market to determine AC charging and discharging schedules. Then, the Intraday market optimization follows, enabling countertrades based on prevailing market conditions. Optimization is performed using the Python-based Pyomo modeling framework and the HiGHS solver Bynum et al., Huangfu and Hall. The proposed scheme achieves reasonable computation times on a commercial 12-core CPU, demonstrating the practical applicability of the modeling approach.

The resulting optimized schedules capture the temporal interaction between household demand, photovoltaic generation, and bidirectional charging decisions. These time-resolved operation patterns form the basis for the mission profiles analyzed in the subsequent scenarios, enabling a detailed assessment of component utilization and lifetime-relevant load conditions.

Table 7
Empirically observed minimum state-of-charge (SoC) set by end users as the threshold for energy feed-in during bidirectional charging (Ostermann et al., 2023).

Minimum SoC range [%]	Relative probability [%]
30–40	6.7
40–50	53.3
50–60	33.3
60–70	6.7

Table 8
Summary of the key characteristics of the BMW i3 bidirectional charging field dataset employed for model validation. Note that the field study employed a DC wallbox, so the maximum AC charging and feed-in power is 10 kW, which differs from the 11 kW listed in Table 3. All other vehicle parameters remain unchanged.

Characteristic	Value
Number of vehicles	18
Vehicle model	BMW i3
Avg. Recorded days per vehicle	261.5
Avg. Minimum SoC (Energy Feedin)	0.50
Max. AC charging power [kW]	10.0
Max. AC feed-in power [kW]	10.0
EEX energy markets	Day-Ahead & Intraday
Field study duration	Dec 2021–Sept 2022

4. Model validation

The validation aims to verify that the simulation framework realistically reproduces the temporal patterns of vehicle availability, charging, and energy exchange observed in the field data, focusing on system-level accuracy rather than component-level effects. For this purpose, a dataset of 18 BMW i3 vehicles from the BDL project is used (Müller et al., 2023; Ostermann et al., 2023), as detailed by Ostermann et al. (2022).

Although the field experiment was conducted using DC wallboxes, the comparison remains valid for AC bidirectional operation, as the underlying charging control and vehicle availability behavior are independent of whether the power conversion electronics are located in the vehicle or in the charging infrastructure. To ensure comparability, the modeled AC charging power of the BMW i3 is set to 10 kW, corresponding to the maximum output of the DC wallbox, while all other vehicle parameters (see Table 3) remain unchanged.

The dataset includes both solar-integrated and bidirectional charging profiles, with the latter marketed through the aggregator NEXT Kraftwerke in the Day-Ahead and Intraday markets between December 2021 and September 2022. The corresponding 2022 electricity price data are used for model validation. Table 7 summarizes the empirically observed minimum state-of-charge (SoC) settings applied by users during bidirectional operation.

Based on these observations, the minimum SoC in the simulations is set to 50%. Table 8 summarizes the average number of recorded days per vehicle and the key simulation parameters. As the BMW i3 vehicles used for validation have smaller battery capacities than most current EVs, a lower minimum SoC (below 0.5) could be applied for larger batteries when normalizing by remaining driving range rather than relative SoC.

To ensure realistic modeling, the simulated home arrival and departure probabilities must align with empirical data, thereby guaranteeing accurate representation of vehicle availability. As shown in Figs. 11 and 12, the main peaks of the measured distributions are well captured by the simulation, while minor deviations likely result from the limited sample size of 18 vehicles. These small discrepancies are consistent with findings from the larger MiD dataset and have negligible impact on overall model accuracy.

The most critical evaluation is whether the proposed modeling approach can accurately predict daily energy transfer, including both charging and feed-in energy. For this analysis, 100 simulation runs involving 18 vehicles were conducted, with the mean and standard deviation subsequently calculated. Table 9 presents this comparison, revealing a strong correlation between simulated and empirical BMW i3 data and thereby confirming the validity of the approach. This high degree of reproduction across arrival, departure, and power profiles ensures that the driving patterns and energy magnitudes remain statistically representative of real-world behavior. While this macroscopic comparison is not a direct temporal validation of individual mission profiles, it ensures that the input stressors for subsequent electro-thermal models are grounded in recorded vehicle field data. Because the stochastic nature of thermal wear-out is inherently driven by these validated power cycles, the reproduction quality of the power profiles serves as a reliable proxy for reliability-relevant stressors.

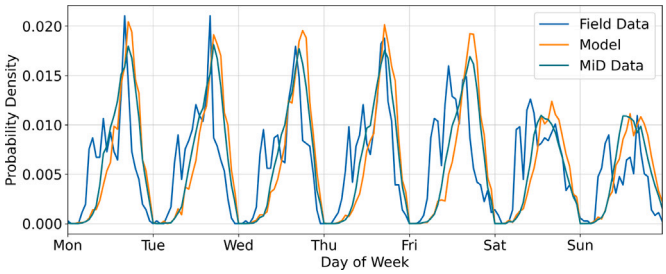

Fig. 11. Comparison of simulated and empirical home arrival probability densities for BMW i3 field data and the MiD dataset. The simulation reproduces the main peaks of real-world arrival behavior, confirming realistic modeling of vehicle availability.

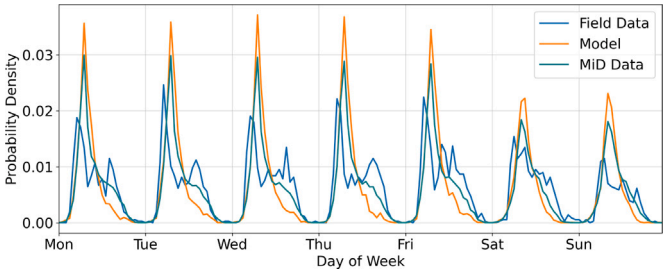

Fig. 12. Comparison of simulated and empirical home departure probability densities for BMW i3 field data and the MiD dataset. The model accurately captures the dominant morning departure peaks, consistent with observed commuter patterns.

Table 9
Comparison of average daily charging and feed-in energy between BMW i3 field data and simulated model data.

Metric	Field Data	Model Data	
	Mean	Mean	Std.
Avg. Daily charging energy [kWh]	15.0	15.0	0.5
Avg. Daily feed-in energy [kWh]	9.0	8.6	0.6

5. Results: Mission profile analysis

This chapter presents the results of the simulation study, focusing on key characteristics of bidirectional AC charging mission profiles and their comparison to unidirectional AC charging profiles. The analysis considers four scenarios. In all scenarios, household base electricity consumption and compensation for solar feed-in are handled via Intraday Market prices, as these cannot be planned in advance like EV charging.

Table 10
Simulation parameters for the results chapter. Two variants are considered: Variant A assumes a large price spread of 233 €/MWh, with feed-in energy compensated only at the EEX market price, while taxes and levies paid on consumption are not reimbursed. Variant B reflects a fully enabled energy trading framework, with the price spread reduced to a trader's markup of 3.5 €/MWh.

Scenario Simulation parameters	
Simulation runs	300
Mobility-profiles	R1: 100x, R3: 100x, R7: 100x
Electric vehicle	Tesla Model 3 LR
Charging modes	AC and DC charging.
AC-charging power	11 kW
AC-feed-in power	11 kW
DC-charging power	108 kW (10%–80% SoC)
AC-charging availability	Daily after the last trip.
Minimum SoC	50% (Energy feed-in into grid)
DC charging cost	0.64 €/kWh
Charging/Feed-in losses	Piecewise linear
Auxiliary losses	100 W
Optimization horizon	3-day sliding window, taking results from day 1.
Target SoC	1.0 (End of optimization horizon)
Ambient temperature	2021 (Stuttgart-Echterdingen)
EV charging costs	2021 Day-Ahead and Intraday.
EV feed-in compensation	2021 Day-Ahead and Intraday.
Household baseload cost	2021 Intraday Market Price
Solar feed-in compensation	2021 Intraday Market Price
Cost-feed-in price spread	**Variant A**: 233 €/MWh, **Variant B**: 3.5 €/MWh.

Unidirectional Reference (U1): Cost-optimal, unidirectional charging of an EV in a household without a solar roof. EV charging costs are determined by Day-Ahead market prices, adjusted for taxes and fees.
Unidirectional Solar (U2): Unidirectional EV charging in a household with a solar roof, optimizing for self-consumption. EV charging costs are based on Day-Ahead market prices, adjusted for taxes and fees.
Bidirectional Day-Ahead (B1): Bidirectional energy exchange between the EV, household, and grid in a household with a solar roof. EV energy exchange costs and renumeration are determined by Day-Ahead market prices, adjusted for taxes and fees.
Bidirectional Intraday (B2): Extends the Bidirectional Day-Ahead scenario with a two-step EV energy exchange optimization. First, Day-Ahead market optimization determines AC charging and discharging schedules. Second, Intraday market optimization allows countertrades while keeping initial Day-Ahead trades.

For both bidirectional charging scenarios, two variants are considered:
Variant A: Large cost-feed-in price spread of 233 €/MWh due to taxes and levies applied to consumption but not reimbursed for feed-in, resulting in a wide price difference.
Variant B: Small spread of 3.5 €/MWh, reflecting only a minor trader margin. Taxes and levies are applied to consumption but not to bidirectional energy exchange.

The year 2021 was selected for energy prices to avoid the distortions caused by the geopolitical crisis in subsequent years. For each of the four scenarios, 300 one-year mission profiles were generated based on the simulation parameters in Table 10. The results are discussed separately for Variants A and B.

The following two subsections present the simulation results for the mission profiles of the unidirectional and bidirectional scenarios. Each mission profile is structured as shown in Fig. 2 and captures the distribution of ambient temperature during charging and discharging events, together with the corresponding power levels and their durations.

5.1. Mission profiles: Unidirectional charging

Fig. 13 shows the mission profiles for the Unidirectional Reference (U1) and Unidirectional Solar (U2) scenarios. The upper panel depicts

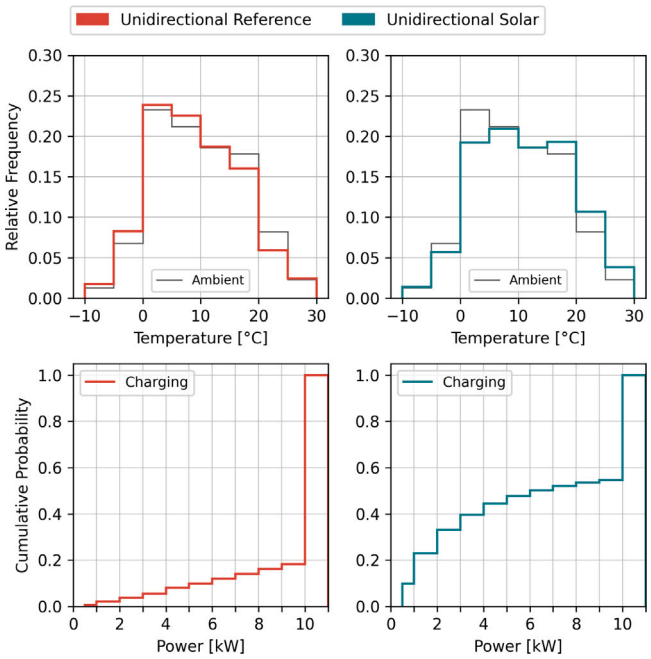

Fig. 13. Main characteristics of the Unidirectional Reference (U1) and Unidirectional Solar (U2) mission profiles: Shown as a reference for comparison with bidirectional mission profiles, with two subplots illustrating (i) the relative ambient temperature distribution of charging and feed-in events versus outdoor temperature, and (ii) cumulative distributions of charging and feed-in power.

the relative frequency of ambient temperatures during charging, and the lower panel shows the cumulative distribution of charging power. Durations are analyzed only for the bidirectional cases (B1, B2), as this section focuses on reference rather than detailed unidirectional profiles. In U1, the ambient temperature distribution during charging mirrors the overall outdoor temperature pattern. In U2, with self-consumption–optimized charging, events shift toward slightly higher temperatures, as solar generation mainly occurs during sunny, warmer periods. A clear difference is also visible in the charging power distribution. In U1, high charging power dominates: over 80% of events occur at the onboard charger's maximum of 11 kW, where efficiency is highest. In contrast, in U2, only about 40% reach 11 kW, as charging follows the PV generation profile, whose peaks are typically well below 11 kW. Consequently, around 40% of events occur below 4 kW, emphasizing the importance of high part-load efficiency in AC onboard chargers for vehicles with solar roofs.

5.2. Mission profiles: Bidirectional charging

Figs. 14 and 15 present the mission profiles for bidirectional scenarios (B1 and B2) for both Variants (A and B). illustrating ambient temperature distributions, power levels and event durations. Together, these distributions define the mission profile and form the basis for a complete lifetime assessment of EV power-electronic components, as illustrated in Fig. 2.

Variant A: Higher Price Spread

In Variant A (Fig. 14), charging and discharging events shift toward higher temperatures. This shift is explained by the large price gap between household consumption and grid feed-in, which discourages feeding energy into the grid and leads the vehicle to prioritize reducing household grid consumption, peaking during the daytime. Over 80% of feed-in events stay below 4 kW to cover base load, whereas charging often occurs at higher power, driven by household demand, rapid SOC recovery, and charger efficiency. Duration-power distributions

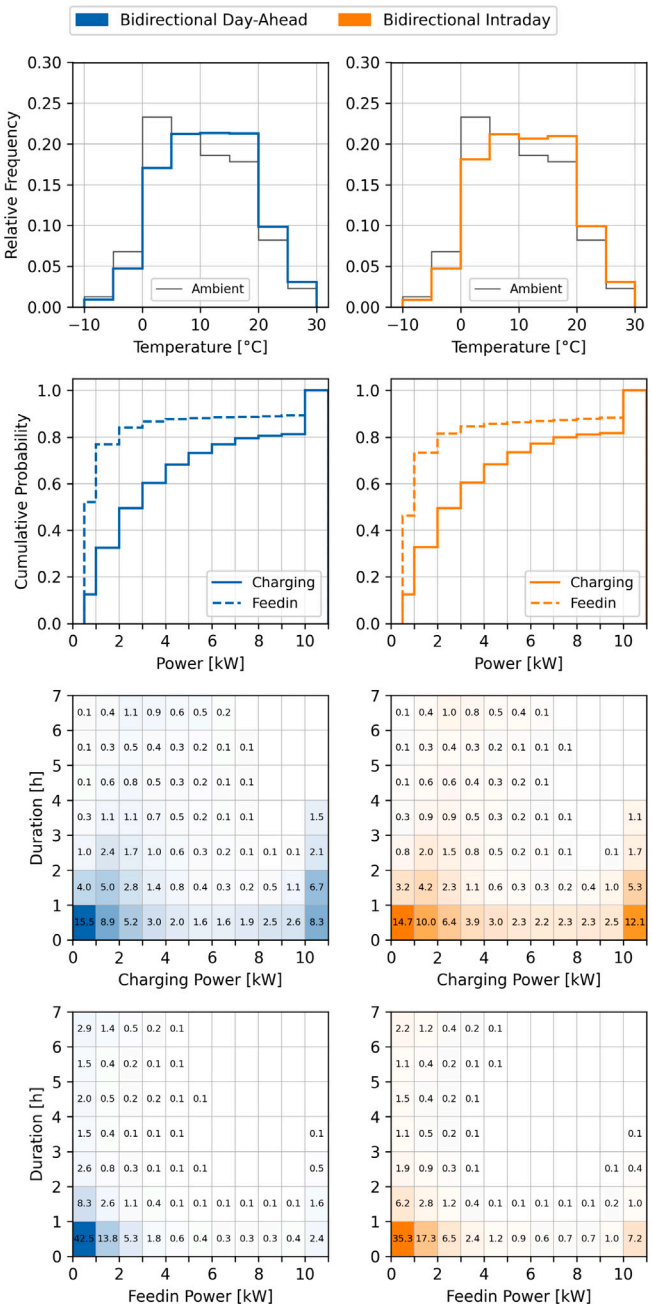

Fig. 14. Variant A: A market scenario with a large cost–feed-in spread of 233 €/MWh, resulting from grid fees and taxes on consumption while feed-in is compensated only at the market price. The mission profile is presented in four subplots: (i) relative ambient temperature distribution of charging and feed-in events compared with outdoor temperature, (ii) cumulative distributions of charging and feed-in power, (iii) event duration versus charging power, and (iv) event duration versus feed-in power.

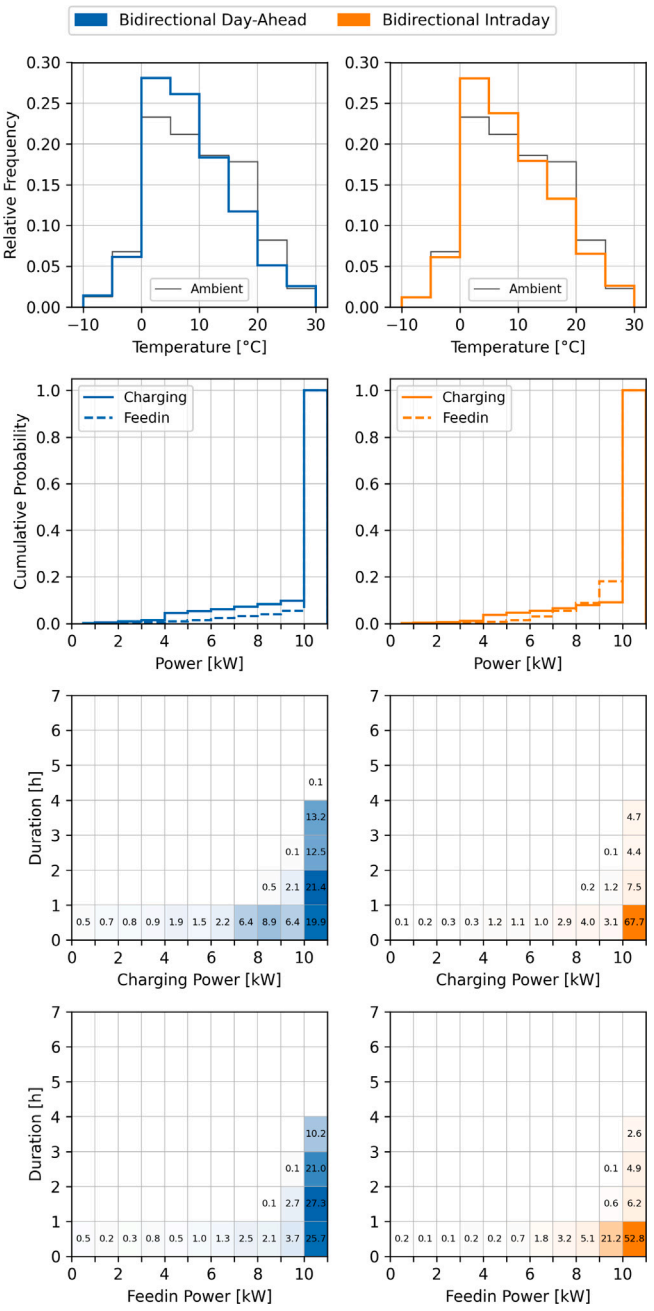

Fig. 15. Variant B: A market scenario with a small cost–feed-in spread of 3.5 €/MWh, reflecting only a trader's markup, with no grid fees or taxes applied to bidirectional energy transfer. The mission profile is presented in four subplots: (i) relative ambient temperature distribution of charging and feed-in events compared with outdoor temperature, (ii) cumulative distributions of charging and feed-in power, (iii) event duration versus charging power, and (iv) event duration versus feed-in power.

show two charging clusters: low power (<4 kW, <2 h) for PV surplus and high power (11 kW, <3 h) for fast SOC recovery or favorable prices. Feed-in, in contrast, forms a single low-power, short-duration cluster. Differences between Day-Ahead and Intraday optimization are minimal, as the large price spread dominates system behavior.

Variant B: Lower Price Spread

In Variant B (Fig. 15), charging and feed-in events shift toward lower temperatures, as larger price variations typically occur during colder months (FfE - Forschungsstelle für Energiewirtschaft e.V., 2022). The small 3.5 €/MWh price spread makes market fluctuations the dominant trigger. High-power events dominate, with up to 90% above 9 kW, reflecting charger efficiency and bidirectional trading in Day-Ahead and Intraday markets. Duration–power distributions show a single high-power cluster (>9 kW) for <4 h in Day-Ahead, and similarly high power but shorter durations (<1 h) in Intraday, reflecting its higher temporal variability.

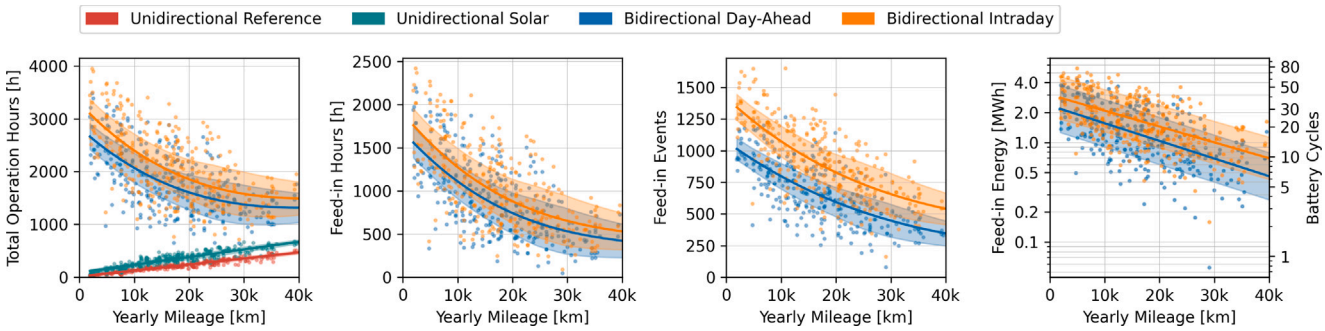

Fig. 16. Variant A: A market scenario with a large cost–feed-in price spread of 233 €/MWh, resulting from grid fees and taxes on consumption while feed-in is compensated only at the market price. The annual operation metrics versus yearly driving distance is presented in four subplots: (i) total operating hours including both charging and feed-in, (ii) feed-in hours only, (iii) the number of feed-in events, and (iv) feed-in energy alongside the associated additional battery cycles for Tesla Model 3 LR.

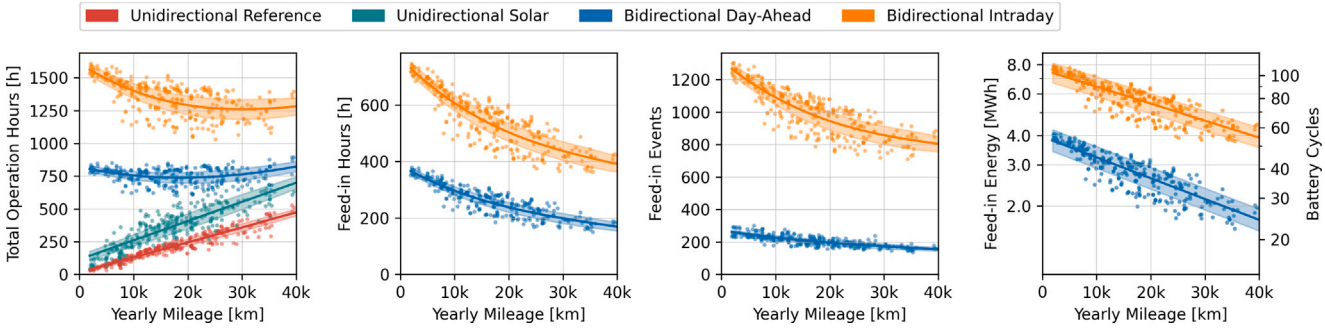

Fig. 17. Variant B: A market scenario with a small cost–feed-in price spread of 3.5 €/MWh, reflecting only a trader's markup, with no grid fees or taxes applied to bidirectional energy transfer. The annual operation metrics versus yearly driving distance is presented in four subplots: (i) total operating hours including both charging and feed-in, (ii) feed-in hours only, (iii) the number of feed-in events, and (iv) feed-in energy alongside the associated additional battery cycles for Tesla Model 3 LR.

5.3. Operating hours, feed-in events, and energy throughput

To gain a comprehensive understanding of the effects of aging, it is essential to consider mission profiles and their effects on additional operating hours, the number of feed-in events, and the total energy exchanged over the vehicle's lifetime. Figs. 16 and 17 show these metrics for variants A and B versus annual driving distance, which strongly affects availability for bidirectional charging. The subplots depict total operating hours, feed-in hours, number of feed-in events, and feed-in energy (or additional battery cycles). For a typical commuter driving 12,000 km/year, the key findings are:

Variant A:

- Approximately 2000 bidirectional operating hours in the Day-Ahead market and 2300 h in the Intraday market, with about 50% of these being feed-in hours.
- Around 750 feed-in events in the Day-Ahead market and 1000 in the Intraday market.
- Total feed-in energy of roughly 2 MWh per year, corresponding to approximately 30 additional battery cycles for the Tesla Model 3 LR. Differences between Day-Ahead and Intraday are small.

Variant B:

- Approximately 750 bidirectional operating hours in the Day-Ahead market and 1300 h in the Intraday market, with roughly 40% being feed-in hours.
- Feed-in events number around 200 in the Day-Ahead market and 1000 in the Intraday market. The huge gap between Day-Ahead and Intraday results represents a major difference compared to Variant A.
- Total feed-in energy reaches about 6 MWh per year in the Intraday market, corresponding to approximately 80 additional battery cycles, and 3 MWh per year in the Day-Ahead market, corresponding to roughly 40 additional cycles. The number of cycles is calculated with respect to the Tesla Model 3 LR battery capacity.

Variant B exchanges more total energy but has fewer feed-in hours, due to its lower charging powers over longer durations. This leads to more operating hours despite less energy exchanged, with implications for onboard charger design: wide cost–feed-in spreads increase operating hours at low power, while narrow spreads favor higher-power, shorter-duration operation. Globally, mission profiles vary with regulatory and economic conditions, e.g., some markets resemble Variant B, others Variant A, highlighting the need for careful component design. While these variants exhibit distinct stress patterns, we intentionally avoid mapping them to specific fatigue models, as the actual damage regime depends on hardware-specific thermal swings (ΔT). In low-power AC bidirectional charging, thermal excursions may remain within the elastic limit of the materials, where standard power-cycling models could overstate degradation without precise data on the converter's thermal resistance (Z_{th}) and packaging. Consequently, this study provides the mission profiles necessary for reliability engineers to apply appropriate damage accumulation models ranging from linear to non-linear once the specific topology and cooling architecture are defined.

Our findings align with previous studies on bidirectional charging and battery aging. Mobilityhouse and RWTH Aachen (The Mobility House and RWTH Aachen University, 2025) report an additional annual throughput of 4.70 MWh, which is within the range covered by our scenarios when accounting for charging energy, feed-in energy, and

losses. In our simulations, annual feed-in energy spans roughly 2 to 6 MWh for a representative commuter, depending on market design and optimization setting, showing a comparable order of magnitude while explicitly resolving scenario-dependent dispersion.

Compared with prior mission-profile-related studies that mainly report aggregate energy and remuneration metrics (Kern et al., 2020; Vollmuth et al., 2024), this work extends benchmarking to reliability-relevant profile descriptors, including power-level distributions, event durations, and operating-hour patterns. The comparison indicates broad consistency in directional trends, while quantitative deviations are expected because of differences in tariff structures, feed-in compensation rules, charging constraints, and vehicle availability assumptions. This explicit benchmarking context improves interpretability and clarifies that reported values should be compared on an assumption-consistent basis rather than as universal constants.

The differences in operating hours and power levels influence the thermal loading and aging of the onboard charger's power electronics. In Variant A, extended operation at low power results in longer dwell times at moderate temperatures, which have limited impact on solder fatigue and interconnect degradation but can contribute to gradual wear of temperature-sensitive components such as electrolytic capacitors. In Variant B, higher power peaks over shorter durations induce stronger thermal cycling, posing a greater risk of solder and interconnect fatigue. Hence, market-driven charging behavior alters not only energy throughput but also the thermal load spectrum relevant for lifetime assessment.

6. Feed-in savings

Following the assessment of component utilization, the next step examines how market-driven charging behavior translates into household feed-in energy and annual cost savings in Variants A and B using the simulation parameters outlined in Table 10. The net savings are considered in addition to those achievable with a solar PV system and thus illustrate the added value of using a bidirectional EV as a mobile battery storage system. Savings are computed solely for participation in the Day-Ahead and Intraday markets, excluding ancillary services, potentially underestimating total savings. Fig. 18 presents the results for Variant A with a large cost–feed-in price spread of 233 €/MWh, while Fig. 19 shows Variant b with a reduced price spread of 3.5 €/MWh. For a representative commuter driving approximately 12,000 km per year, the following net savings can be obtained:

- **Variant A:** With an annual feed-in energy of 2 MWh, net savings of about 150 €/year are achieved. Differences between the Day-Ahead and Intraday markets remain small due to the large cost–feed-in price spread. Although the figure seems to indicate lower savings in the Intraday market, this is only a visual effect. For the same EV, feed-in energy is actually higher in the Intraday market than in the Day-Ahead market, causing the datapoints for a given EV to appear at different x-coordinates.
- **Variant B:** With an annual feed-in energy of 3 MWh in the Day-Ahead market, net savings reach about 200 €/year. In combined Day-Ahead and Intraday operation, the feed-in energy increases to 6 MWh per year, resulting in net savings of roughly 300 €/year.

7. Sensitivity analysis

To evaluate the impact of varying simulation parameters, a sensitivity analysis is conducted. Table 11 lists the modified parameters together with their default values. The analysis investigates variations in the minimum SoC threshold for AC feed-in, vehicle model, charging strategy, annual energy prices, auxiliary losses, and the maximum AC feed-in power. Results are shown in Fig. 20 for Variant A, with a large cost–feed-in spread of 233 €/MWh, and in Fig. 21 for Variant B, with a small spread of 3.5 €/MWh. For the analysis, driving profiles with an annual mileage between 10,000 and 15,000 km are selected. The key findings are summarized as follows:

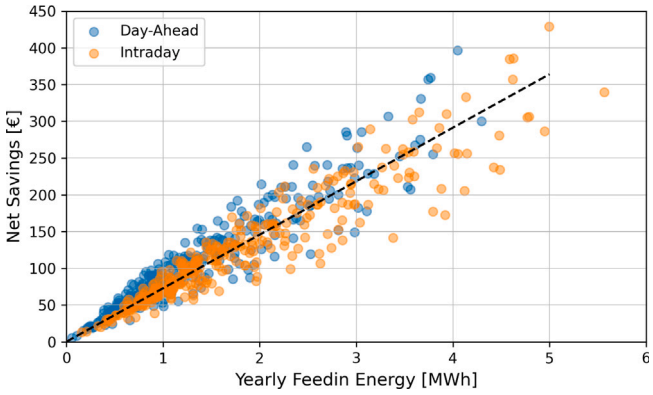

Fig. 18. Variant A: Annual net savings with respect to yearly feed-in energy for the market scenario with a large cost–feed-in spread of 233 €/MWh. The net savings are considered in addition to those achievable with a solar PV system and thus illustrate the added value of a bidirectional EV instead of a stationary battery storage device.

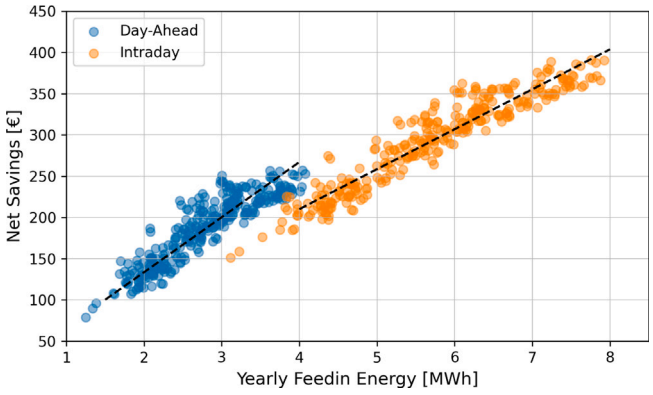

Fig. 19. Variant B: Annual net savings with respect to yearly feed-in energy for the market scenario with a small cost–feed-in spread of 3.5 €/MWh. The net savings are considered in addition to those achievable with a solar PV system and thus illustrate the added value of a bidirectional EV instead of a stationary battery storage device.

- **Minimum SoC:** The minimum SoC threshold for AC feed-in plays only a minor role in Variant A, since self-consumption maximization is the primary objective and trading on the energy markets is limited. In this case, the EV's battery capacity is more than sufficient, so adjustments to the minimum SoC have little effect. In Variant B, however, where active market trading is the focus, the minimum SoC becomes a decisive factor. Lowering the threshold from 50% to 30% increases feed-in energy by about 20%, while raising it to 70% reduces feed-in energy by around 35%.
- **Vehicle Model:** The feed-in energy does not increase significantly when switching from the Tesla Model 3 LR to the Tesla Model S LR Plus (B2), despite its 36% larger 98 kWh HV battery, because self-consumption optimization in Variant A does not depend heavily on large battery capacities. In Variant B, where active energy trading is the focus, battery capacity plays a major role. The Tesla Model 3 SR Plus (B1), with a battery 32% smaller than the default, achieves 30% less feed-in energy. Conversely, the 36% larger 98 kWh HV battery of the Tesla Model S LR Plus (B2) results in a 55% increase in feed-in energy.
- **Charging Strategy:** The results clearly show that the charging strategy and the resulting vehicle availability play a crucial role in determining AC feed-in energy. When the vehicle is only plugged

Table 11
Simulation parameters and their default values used in the sensitivity analysis. The analysis explores variations in SoC threshold, vehicle model, charging strategy, annual energy prices, auxiliary losses, and maximum AC feed-in power. Results are presented in Figs. 20 and 21 for Variant A (large cost–feed-in pice spread) and Variant B (small cost-feed-in price spread), respectively.

Parameter	Default	Variation
Minimum SoC	50%	30% (A1), 70% (A2)
Vehicle model	Tesla Model 3 LR	Tesla Model 3 SR Plus (B1), Tesla Model S LR Plus (B2)
Charging strategy	At Home, after last trip	Weekend at Home (C1), after last trip (C2)
Energy market	Day-Ahead 2021	Day-Ahead 2024 (D1)
Auxiliary losses	100 W	300 W (E1), 0 W (E2)
Max. AC Feed-in Power	11 kW	3.7 kW (F1), 7.2 kW (F2)

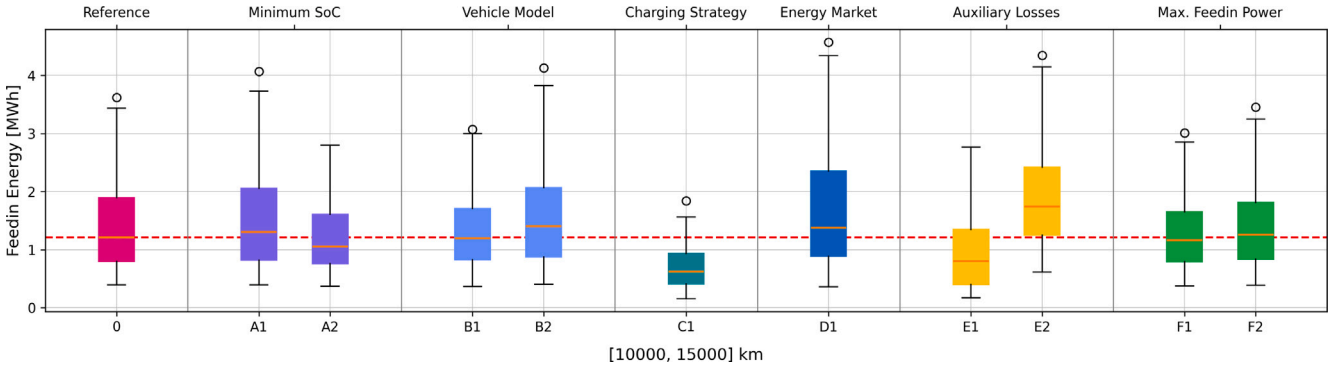

Fig. 20. Variant A: Sensitivity analysis for annual feed-in energy for a market scenario with a large cost–feed-in price spread of 233 €/MWh, resulting from grid fees and taxes on consumption while feed-in is compensated only at the market price. The analysis considers yearly driving distances between 10,000 km and 15,000 km. Charging strategy and auxiliary losses are identified as the most influential factors.

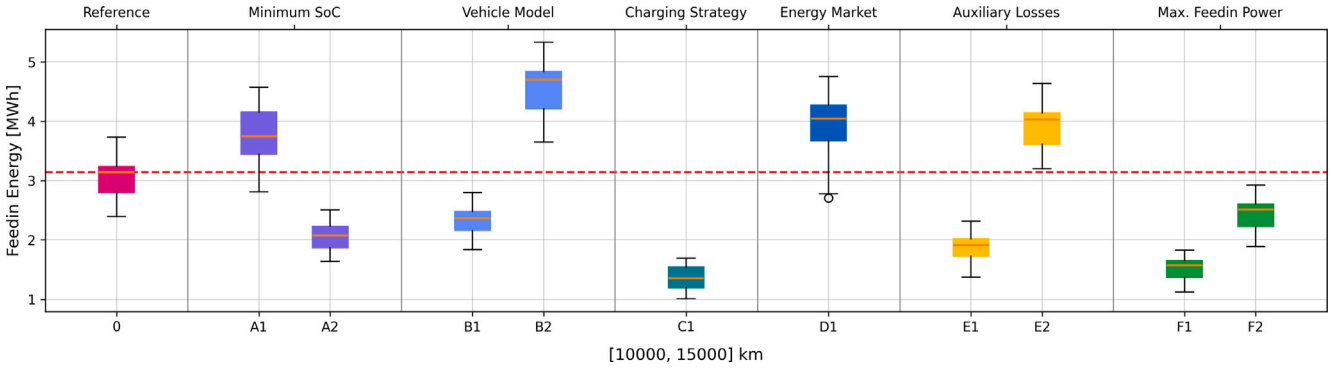

Fig. 21. Variant B: Sensitivity analysis for annual feed-in energy for a market scenario with a small cost–feed-in price spread of 3.5 €/MWh, reflecting only a trader's markup, with no grid fees or taxes applied to bidirectional energy transfer. The analysis considers yearly driving distances between 10,000 km and 15,000 km. In this scenario, all factors exert a comparably strong influence, as the actively tradable energy depends on multiple interacting parameters. These results highlight that outcomes in active trading scenarios must be carefully interpreted in the context of the chosen simulation parameters.

in on weekends after the final trip (C1), AC feed-in energy in Variant A decrease by up to 45%, while feed-in energy in Variant B is reduced by up to 55%. This reduction is caused by the vehicle being less frequently connected, which limits self-consumption optimization in Variant A and active energy trading in Variant B. This underlines that real-world charging behavior, where vehicles are not always connected daily, can substantially reduce the yearly feed-in energy. It also highlights the importance of interpreting published figures on potential revenues and feed-in energy in the context of the assumed vehicle availability.

- **Energy Market:** Daily fluctuations in energy prices have a pronounced effect on AC feed-in energy in Variant B, where market trading is more influential due to the small cost–feed-in price spread. In the 2024 Day-Ahead market (D1), the higher average daily standard deviation of 0.037 €/kWh, compared to 0.029 €/kWh in the 2021 default scenario, leads to an increase in feed-in energy of approximately 29% in Variant B. In Variant A, however, the effect is limited, as self-consumption optimization dominates and variations in market prices have little impact.
- **Auxiliary Losses:** Variations in auxiliary losses have a substantial impact in both Variant A and Variant B. Increasing auxiliary losses from 100 W to 300 W reduces feed-in energy by 35% in Variant A and 40% in Variant B. Conversely, when auxiliary losses are neglected and set to 0 W, feed-in energy increases by 54% in Variant A and 30% in Variant B. This finding is particularly important, as many studies consider only AC conversion efficiency while neglecting auxiliary loads such as coolant pumps, charging communication controllers, and control units. In self-consumption optimization scenarios, neglecting auxiliary losses leads to a significant overestimation of benefits, as the EV frequently operates at part-load, where real system losses are higher than assumed. Overall, the results indicate that minimizing auxiliary losses should be a priority for vehicle manufacturers to fully realize the potential of bidirectional charging.

- **Maximum Feed-in Power:** The EVs maximum AC feed-in power has a significant impact in Variant B, while it has little to no effect in Variant A. In Variant A, self-consumption optimization predominantly occurs at power levels below 3.7 kW, so the feed-in limit does not influence outcomes. In Variant B, where energy trading is the primary driver, the maximum feed-in power strongly affects annual feed-in energy: limiting it to 3.7 kW (F1) reduces feed-in by 52%, while a limit of 7.2 kW results in a 20% reduction. Such limitations are realistic, as grid operators may impose feed-in caps to prevent network overload during periods of high simultaneous injection.

The results demonstrate that SoC limits, auxiliary losses, and grid constraints are the main drivers of system sensitivity and must be precisely modeled for reliable lifetime and economic assessments. Results also highlight that outcomes in active trading scenarios (Variant B) depend on multiple interacting parameters, necessitating careful interpretation within the context of chosen simulation parameters.

8. Summary and conclusion

This study developed and analyzed detailed mission profiles for bidirectional AC charging of EVs, providing a foundation for subsequent investigations into lifetime effects on power electronic components, such as the AC onboard charger. The simulation model was validated against real-world field data and demonstrated high reproduction quality.

Mission profiles were generated for multiple households with an EV and a solar roof under two scenarios. Variant A, characterized by a large cost–feed-in price spread of 233 €/MWh, resulting from grid fees and taxes on consumption while feed-in is compensated only at the market price, making energy feed-in into the grid often economically unattractive. Variant B, by contrast, features a small cost–feed-in spread of 3.5 €/MWh, represents a market-focused environment with minimal markups, where bidirectional energy feed-in into the grid becomes economically attractive. For both scenarios, the optimization of bidirectional energy exchange was conducted for participation in the Day-Ahead market as well as in a combined Day-Ahead and Intraday market setting.

Our results show that in Variant A, self-consumption optimization dominates bidirectional energy exchange, with feed-in occurring predominantly at low power levels and annual feed-in energy reaching 2–3 MWh. In contrast, Variant B is governed by market-driven energy trading, characterized by short, high-power feed-in periods that yield annual feed-in energies of approximately 4 MWh in the Day-Ahead market and up to 8 MWh when combining Day-Ahead and Intraday optimization. The analysis further demonstrates that bidirectional charging substantially increases the total operating hours and switching events of power-electronic components, with a strong dependence on annual driving distance and the resulting vehicle availability. The mission profiles are presented with high fidelity, accurately capturing key operational characteristics and providing a robust foundation for direct use in lifetime assessments of specific EV power-electronic components.

Beyond the development of mission profiles, the economic potential of bidirectional charging was assessed by comparing a bidirectional EV to a stationary battery storage system, representing the added value on top of benefits already achievable through smart charging or self-consumption from a solar roof. For a typical commuter with an annual driving distance of 12,000 km, Variant A yields net savings of approximately 150 €/year, whereas Variant B achieves 200 €/year with Day-Ahead optimization and 300 €/year when combining Day-Ahead and Intraday optimization. It should be noted that the reported annual net savings represent the gross economic benefit derived from market participation and self-consumption. A comprehensive techno-economic lifecycle assessment would further need to internalize the incremental costs of hardware degradation. These include the potential for increased initial CAPEX required to upgrade power-electronic components for extended operating hours—and the risk of shortened service intervals. Consequently, the savings identified in this study define the gross economic potential for bidirectional operation, providing a benchmark for the maximum allowable costs associated with enhanced design margins and extended component service lives, based on the energy price fluctuations of the German electricity market.

A sensitivity analysis revealed that battery state of charge limits, vehicle availability, assumptions on auxiliary losses from cooling and communication controllers, and maximum feed-in power constraints imposed by grid operators have a substantial impact on annual feed-in energy. The vehicle model, the corresponding available battery capacity, and annual electricity market price fluctuations are primarily relevant in Variant B, where active energy trading is enabled by the small cost-feed-in price spread.

Despite the comprehensive simulation and validation workflow, several limitations should be considered when interpreting the results. First, behavioral inputs are derived from historical mobility and household datasets, so structural shifts in mobility demand and household electrification may affect absolute future values. Second, market outcomes depend on the selected regulatory and price assumptions, which vary across countries and over time. Third, infrastructure and operation assumptions, such as charging availability and feed-in constraints, influence achievable operating hours and energy exchange. To ensure the technical rigor of the generated mission profiles, DC fast-charging sessions were explicitly integrated into the simulation framework. This modeling choice prevents a significant overestimation of annual AC operating hours and energy throughput, as long-distance mobility demand is realistically met by DC infrastructure rather than the AC on-board charger. To investigate the cumulative effect on the HV battery, a superposition of high-stress DC fast-charging sessions and the bidirectional AC charging cycles is required to accurately capture these distinct operational regimes. Finally, while the generated mission profiles are suitable as reliability-model inputs, quantitative lifetime conclusions cannot be generalized without calibrated component-specific electro-thermal modeling.

The developed mission profiles are relevant to a wide range of stakeholders. For OEMs and component developers, they provide essential input for the design and qualification of onboard chargers, enabling more accurate estimation of thermal loads, operating hours, switching stresses, and cumulative degradation. Grid operators can use the mission profiles and sensitivity analysis results to focus their modeling on the most critical parameters and assess the impact of bidirectional EV charging on distribution networks. Policymakers and regulators can use these results to evaluate various feed-in compensation schemes, supporting the efficient and reliable integration of bidirectional EV charging. Overall, the results highlight that bidirectional charging requires careful design of components, effective thermal management, and optimized control strategies to mitigate aging effects. Fully realizing these benefits requires a holistic approach that balances economic incentives with the limitations imposed by component longevity. Future research should apply the developed mission profiles to onboard charger lifetime models, incorporate real-world degradation data, and develop control strategies that optimize both profitability and component durability.

CRediT authorship contribution statement

Stefan Schmalzl: Writing – review & editing, Writing – original draft, Visualization, Validation, Methodology, Investigation, Formal analysis, Data curation, Conceptualization. **Michael von Bonin:** Writing – review & editing, Methodology, Conceptualization. **Michael Frey:** Writing – review & editing, Supervision, Project administration. **Frank Gauterin:** Writing – review & editing, Supervision. **Martin Braun:** Writing – review & editing, Methodology.

Declaration of Generative AI and AI-assisted technologies in the writing process

Any use of generative AI in this manuscript adheres to ethical guidelines for the use and acknowledgment of generative AI in academic research and was solely used to enhance the readability and language of the work.

Declaration of competing interest

The authors declare that they have no known competing financial interests or personal relationships that could have appeared to influence the work reported in this paper.

Acknowledgments

This work was supported by the German Federal Ministry for Economic Affairs and Climate Action (BMWK) under the projects “EMob-Cold+V2G” (grant number 16EM7001) and “Ladeinfrastruktur 2.0” (grant number 0350048D). Each author has made a substantial contribution to the work, which has been thoroughly vetted for accuracy and assumes responsibility for the integrity of their contributions.

Data availability

The authors do not have permission to share data.

References

Banol Arias, N., Hashemi, S., Andersen, P.B., Traeholt, C., Romero, R., 2019. Distribution system services provided by electric vehicles: Recent status, challenges, and future prospects. IEEE Trans. Intell. Transp. Syst. 20 (12), 4277–4296. http://dx.doi.org/10.1109/tits.2018.2889439.

BDEW Bundesverband der Energie- und Wasserwirtschaft e.V., 2025. Standardlastprofile strom. Available at: https://www.bdew.de/energie/standardlastprofile-strom/. (Accessed 02 January 2025).

Blaabjerg, F., Wang, H., Vernica, I., Liu, B., Davari, P., 2021. Reliability of power electronic systems for EV/HEV applications. Proc. IEEE 109 (6), 1060–1076. http://dx.doi.org/10.1109/jproc.2020.3031041.

Böttger, D., Dreher, A., Ganal, I., Gauglitz, P., Geiger, D., Gerlach, A.-K., Gerhardt, N., Harms, Y., Härtel, P., Knorr, K., Jentsch, M., Mende, D., Pfennig, M., Schmitz, R., Stappel, M., Bonin, M.v., 2019. Systemkontext: Modellbildung für nationale energieversorgungsstrukturen im europäischen kontext unter besonderer berücksichtigung der zulässigkeit von vereinfachungen und aggregationen. http://dx.doi.org/10.24406/PUBLICA-FHG-300439.

Bynum, M.L., Hackebeil, G.A., Hart, W.E., Laird, C.D., Nicholson, B.L., Siirola, J.D., Watson, J.-P., Woodruff, D.L., 2021. Pyomo — Optimization Modeling in Python. Springer International Publishing, http://dx.doi.org/10.1007/978-3-030-68928-5.

Chakraborty, S., Hasan, M.M., Paul, M., Tran, D.-D., Geury, T., Davari, P., Blaabjerg, F., Baghdadi, M.E., Hegazy, O., 2022. Real-life mission profile-oriented lifetime estimation of a SiC interleaved bidirectional HV dc/DC converter for electric vehicle drivetrains. IEEE J. Emerg. Sel. Top. Power Electron. 10 (5), 5142–5167. http://dx.doi.org/10.1109/jestpe.2021.3083198.

Dargahi, A., Ploix, S., Soroudi, A., Wurtz, F., 2014. Optimal household energy management using V2H flexibilities. COMPEL - Int. J. Comput. Math. Electr. Electron. Eng. 33 (3), 777–792. http://dx.doi.org/10.1108/COMPEL-10-2012-0223.

De León-Aldaco, S.E., Calleja, H., Chan, F., Jiménez-Grajales, H.R., 2013. Effect of the mission profile on the reliability of a power converter aimed at photovoltaic applications—A case study. IEEE Trans. Power Electron. 28 (6), 2998–3007. http://dx.doi.org/10.1109/tpel.2012.2222673.

Dubarry, M., Devie, A., McKenzie, K., 2017. Durability and reliability of electric vehicle batteries under electric utility grid operations: Bidirectional charging impact analysis. J. Power Sources 358, 39–49. http://dx.doi.org/10.1016/j.jpowsour.2017.05.015.

DWD, 2025. Open data, station ID: 4931, stuttgart-echterdingen. Available at: https://opendata.dwd.de/climate_environment/CDC/observations_germany/climate/hourly/air_temperature/. (Accessed 02 October 2024).

EEX, 2025. Market data hub. https://www.eex.com/en/market-data. (Accessed 01 July 2025).

Electric Vehicle Database, 2025. Current and upcoming electric vehicles. URL: https://ev-database.org/.

FfE - Forschungsstelle für Energiewirtschaft e.V., 2022. German Electricity Prices on the EPEX Spot Exchange in 2021. Technical Report, FfE - Forschungsstelle für Energiewirtschaft e.V., Available online: https://www.ffe.de/en/publications/german-electricity-prices-on-the-epex-spot-exchange-in-2021/. (Accessed 03 September 2025).

for Solar Energy Systems ISE, F.I., 2024. Recent Facts about Photovoltaics in Germany. Technical Report, Fraunhofer ISE, Freiburg, Germany, URL: https://www.ise.fraunhofer.de/content/dam/ise/en/documents/publications/studies/recent-facts-about-photovoltaics-in-germany.pdf (Accessed October 2025).

Gong, J., Wasylowski, D., Figgener, J., Bihn, S., Rücker, F., Ringbeck, F., Sauer, D.U., 2024. Quantifying the impact of V2X operation on electric vehicle battery degradation: An experimental evaluation. ETransportation 20, 100316. http://dx.doi.org/10.1016/j.etran.2024.100316.

Hirschmann, D., Tissen, D., Schroder, S., De Doncker, R.W., 2007. Reliability prediction for inverters in hybrid electrical vehicles. IEEE Trans. Power Electron. 22 (6), 2511–2517. http://dx.doi.org/10.1109/tpel.2007.909236.

Huangfu, Q., Hall, J.A.J., 2017. Parallelizing the dual revised simplex method. Math. Program. Comput. 10 (1), 119–142. http://dx.doi.org/10.1007/s12532-017-0130-5.

Infas Institut für Sozialwissenschaft, 2018. Mobilität in deutschland. http://www.mobilitaet-in-deutschland.de.

Infas Institut für Sozialwissenschaft, 2023. Mobilität in deutschland. http://www.mobilitaet-in-deutschland.de.

International Energy Agency (IEA), 2025. Global EV outlook 2025. URL: https://www.iea.org/reports/global-ev-outlook-2025. (Accessed 12 September 2025).

Kardan, F., Shekhar, A., Bauer, P., 2023. End-of-life comparison of full-bridge and half-bridge DC/DC converter switches used for EV charging. In: IECON 2023-49th Annual Conference of the IEEE Industrial Electronics Society. IEEE, pp. 1–6. http://dx.doi.org/10.1109/iecon51785.2023.10312649.

Kern, T., Dossow, P., Morlock, E., 2022. Revenue opportunities by integrating combined vehicle-to-home and vehicle-to-grid applications in smart homes. Appl. Energy 307, 118187. http://dx.doi.org/10.1016/j.apenergy.2021.118187.

Kern, T., Dossow, P., von Roon, S., 2020. Integrating bidirectionally chargeable electric vehicles into the electricity markets. Energies 13 (21), 5812. http://dx.doi.org/10.3390/en13215812.

Kim, I., Park, J.-W., 2024. Multifunctional integrated DC–DC converter for electric vehicles. IEEE Trans. Power Electron. 39 (6), 7252–7263. http://dx.doi.org/10.1109/tpel.2024.3378278.

Koncar, I., Bayram, I.S., 2021. A probabilistic methodology to quantify the impacts of cold weather on electric vehicle demand: A case study in the U.K.. IEEE Access 9, 88205–88216. http://dx.doi.org/10.1109/access.2021.3090534.

Lenz, J.M., Sartori, H.C., Pinheiro, J.R., 2017. Mission profile characterization of PV systems for the specification of power converter design requirements. Sol. Energy 157, 263–276. http://dx.doi.org/10.1016/j.solener.2017.08.020.

Lienig, J., Bruemmer, H., 2017. Fundamentals of Electronic Systems Design. Springer International Publishing, http://dx.doi.org/10.1007/978-3-319-55840-0.

Ma, K., Liserre, M., Blaabjerg, F., Kerekes, T., 2015. Thermal loading and lifetime estimation for power device considering mission profiles in wind power converter. IEEE Trans. Power Electron. 30 (2), 590–602. http://dx.doi.org/10.1109/tpel.2014.2312335.

Miner, M.A., 1945. Cumulative damage in fatigue. J. Appl. Mech. 12 (3), A159–A164. http://dx.doi.org/10.1115/1.4009458.

Müller, M., Kern, T., Ostermann, A., Dossow, A., 2023. BDL — Bidirektionales Lademanagement: Abschlussbericht Der Ffe. Technical Report, Forschungsstelle für Energiewirtschaft (FfE), http://dx.doi.org/10.34805/ffe-08-23, URL: https://openaccess.ffe.de/10.34805/ffe-08-23/, Open Access report.

Nagler, R., 2021. Standing Still: The Utilization of Private Cars in Everyday Life. RAC Foundation, https://www.racfoundation.org/wp-content/uploads/standing-still-Nagler-June-2021.pdf. (Accessed 14 September 2025).

Novak, M., Sangwongwanich, A., Blaabjerg, F., 2020. Monte Carlo based reliability estimation methods in power electronics. In: 2020 IEEE 21st Workshop on Control and Modeling for Power Electronics. COMPEL, IEEE, pp. 1–7. http://dx.doi.org/10.1109/compel49091.2020.9265685.

Ostermann, A., Haug, T., Hinterstocker, M., Hahne, H., 2023. Bidirectional electric vehicles field trial data set. In: NEIS 2023 - Conference on Sustainable Energy Supply and Energy Storage Systems. NEIS, Hamburg, Germany.

Ostermann, A., Haug, T., Regener, V., 2022. Analysis of the intraday use case in the field trial of the bidirectional charging management project. In: 6th E-Mobility Power System Integration Symposium. EMOB 2022, Vol. 2022, pp. 42–49. http://dx.doi.org/10.1049/icp.2022.2714.

Pham, P.H., Nabih, A., Wang, S., Li, Q., 2022. 11-kW high-frequency high-density bidirectional OBC with PCB winding magnetic design. In: 2022 IEEE Applied Power Electronics Conference and Exposition. APEC, Houston, TX, USA, pp. 1176–1181. http://dx.doi.org/10.1109/APEC42165.2022.9773481.

Polat, H., Hosseinabadi, F., Chakraborty, S., et al., 2023. Assessing the impact of EV charging and discharging profiles on T-type active front end charger lifetime. In: IECON 2023 - 49th Annual Conference of the IEEE Industrial Electronics Society. pp. 1–7. http://dx.doi.org/10.1109/IECON51785.2023.10312263.

Popolizio, F., Wik, T., Lee, C.F., Zou, C., 2025. Nonlinear online optimization for vehicle-home-grid integration including household load prediction and battery degradation. http://dx.doi.org/10.48550/arXiv.2504.09657, URL: https://arxiv.org/abs/2504.09657, arXiv preprint arXiv:2504.09657, Submitted to the 2025 IEEE Conference on Decision and Control (CDC).

Pradhan, R., Keshmiri, N., Emadi, A., 2023. On-board chargers for high-voltage electric vehicle powertrains: Future trends and challenges. IEEE Open J. Power Electron. 4, 189–207. http://dx.doi.org/10.1109/ojpel.2023.3251992.

Purkus, A., Schwarz, C., Reuter, M., Resch, G., 2015. Market integration of renewable energies through direct marketing – lessons learned from the german market premium scheme. Energy Sustain. Soc. 5 (1), 1–13. http://dx.doi.org/10.1186/s13705-015-0040-1, URL: https://energsustainsoc.biomedcentral.com/articles/10.1186/s13705-015-0040-1.

Rodriguez, C., Vidal, C., Diaz, M., Contreras, E., Guggisberg, G., Rivas, I., 2021. An overview of challenges and benefits associated to the development of vehicle to grid technology. In: 2021 IEEE CHILEAN Conference on Electrical, Electronics Engineering, Information and Communication Technologies. CHILECON, IEEE, pp. 1–6. http://dx.doi.org/10.1109/chilecon54041.2021.9702991.

Sagaria, S., van der Kam, M., Boström, T., 2025. Vehicle-to-grid impact on battery degradation and estimation of V2G economic compensation. Appl. Energy 377, 124546. http://dx.doi.org/10.1016/j.apenergy.2024.124546.

Soldati, A., Pietrini, G., Dalboni, M., Concari, C., 2018. Electric-vehicle power converters model-based design-for-reliability. CPSS Trans. Power Electron. Appl. 3 (2), 102–110. http://dx.doi.org/10.24295/cpsstpea.2018.00010.

The Mobility House and RWTH Aachen University, 2025. RWTH aachen study confirms: Bidirectional charging hardly affects the lifespan of electric vehicle batteries. URL: https://www.mobilityhouse.com/int_en/our-company/newsroom/article/aachen-studie-tmh-eng. (Accessed 04 October 2025).

Tjaden, T., Bergner, J., Weniger, J., Quaschning, V., 2015. Repräsentative elektrische lastprofile für wohngebäude in deutschland auf 1-sekündiger datenbasis. http://dx.doi.org/10.13140/RG.2.1.5112.0080/1.

Vollmuth, P., Wohlschlager, D., Wasmeier, L., Kern, T., 2024. Prospects of electric vehicle V2G multi-use: Profitability and GHG emissions for use case combinations of smart and bidirectional charging today and 2030. Appl. Energy 371, 123679. http://dx.doi.org/10.1016/j.apenergy.2024.123679.

Wouters, H., Martinez, W., 2024. Bidirectional onboard chargers for electric vehicles: State-of-the-art and future trends. IEEE Trans. Power Electron. 39 (1), 693–716. http://dx.doi.org/10.1109/tpel.2023.3319996.

Yang, S., Bryant, A., Mawby, P., Xiang, D., Ran, L., Tavner, P., 2009. An industry-based survey of reliability in power electronic converters. In: 2009 IEEE Energy Conversion Congress and Exposition. IEEE, pp. 2612–2618. http://dx.doi.org/10.1109/ecce.2009.5316356.

Yilmaz, M., Krein, P.T., 2012. Review of benefits and challenges of vehicle-to-grid technology. In: 2012 IEEE Energy Conversion Congress and Exposition. ECCE, IEEE, pp. 3082–3089. http://dx.doi.org/10.1109/ecce.2012.6342356.

Zhou, D., Song, Y., Liu, Y., Blaabjerg, F., 2019. Mission profile based reliability evaluation of capacitor banks in wind power converters. IEEE Trans. Power Electron. 34 (5), 4665–4677. http://dx.doi.org/10.1109/tpel.2018.2865710.